Sensitivity of Electroslag Weld Metal to Hydrogen

Hydrogen-charged tensile specimens of weld metal show that maximum embrittlement is caused by grain boundary separation mode

BY L. N. PUSSEGODA AND W. R. TYSON

ABSTRACT. The susceptibility of electroslag weld metal to hydrogen has been studied by slow tensile testing and metallographic examination of fractured specimens from a weldment of ASTM A36 steel plate. With constant hydrogen concentration, three distinct hydrogen-assisted fracture modes were observed. The first at low temperatures was "quasi-cleavage." As the temperature was increased, the second consisted of prior-austenite grain-boundary separations, and then microvoid—the third mode—coalescence occurred.

The embrittlement index is largest for the grain-boundary separation mode. Both the temperature of maximum embrittlement and the upper limit of the temperature range for embrittlement depend on hydrogen content, increasing from −10 and 55°C (14 and 131°F) respectively at 1 ppm to 30 and 145°C (86 and 293°F) at 3 ppm. The presence of internal hydrogen increases both the yield and flow stresses at temperatures where hydrogen embrittlement occurs.

Grain boundary separations which occur in electroslag weldments are discussed. It is concluded that these are a result of hydrogen-induced cracks in a microstructure which provides a crack path prone to low-energy fracture.

Introduction

Internal hydrogen embrittlement of weldments appears in the form of "cold cracks" (a form of delayed failure due to hydrogen) either in the weld metal or heat affected zone (HAZ). The following factors play a major role in the formation of cold cracks:

1. A residual tensile stress on the weldment.
2. Sufficient hydrogen introduced during welding.
3. A susceptible microstructure.

The susceptibility of steels to hydrogen embrittlement generally increases with strength level, and cold cracking is usually associated with hard microstructures in welds. For example, it is well known that martensites crack, and this tendency increases with carbon content and hardness (Ref. 1). However, the microstructure also has an effect on hydrogen susceptibility in steels of the same hardness (Ref. 2). Therefore, it is not always possible to use steels with a low strength and softer microstructure, because some are susceptible to hydrogen-induced failure in spite of their low hardness (Ref. 3).

Small cracks in electroslag welds (ESW) which were observed recently both in the field and laboratory may be a result of a soft and susceptible microstructure (Ref. 4-7). In general, the hydrogen level at temperatures when cold cracks form is expected to be very low in these high heat input welds. The cracks in ESW metal have been observed almost entirely in the proeutectoid ferrite network which outlines the prior-austenite grain-boundaries, and hence are referred to as grain-boundary separations. It has been shown that these grain-boundary separations are hydrogen-induced cracks and that the critical hydrogen content for the occurrence of such separations is a function of both restraint and cooling rate of the weldment (Ref. 5-7). Similar cracks along the prior-austenite grain-boundaries, have been frequently observed in weld metal microstructures which simulate those found in arc welds (Ref. 1).

The discovery of hydrogen-induced cracks in ESW metal caused concern about the use of electroslag welding for critical applications such as tension members in bridges (Ref. 4). To make this economical welding process sufficiently reliable for such critical applications, the effect of variables such as hydrogen content, microstructure, and residual stress in the grain-boundary separation mechanism should be measured.

The purpose of the present study of the sensitivity to hydrogen of ESW metal was:

1. To determine hydrogen levels required to cause ductility loss in weld metal as a function of temperature, and
2. To study fracture paths and failure modes in an attempt to identify embrittlement mechanisms.

L. N. PUSSEGODA is Post-Doctoral Fellow, Metallurgy Section, and W. R. TYSON is Head, Engineering and Metal Physics Section, Physical Metallurgy Research Laboratories, CANMET, Department of Energy, Mines and Resources, Ottawa, Canada.

Experimental Procedures

Materials

The ESW metal used in this study was cut from a weldment made in the laboratory of the Dominion Bridge Co., Canada. The weld joined ASTM A36 steel plates 64 mm (2.5 in.) thick with a weld gap of 25 mm (1 in.) using an AWS EH14-EW electroslag electrode and Linde 125 flux (dry) in a dry atmosphere. Welding current and voltage were 600 amperes (A) and 40 volts (V), respectively. The chemical composition and mechanical properties of the weld metal are given in Table 1.

Specimen Preparation

Miniature Hounsfield tensile specimens of gauge diameter 3 mm (0.126 in.) were machined from the weld metal at locations shown in Fig. 1. The tensile axis of each specimen was in the welding direction.

Cathodic Charging and Hydrogen Analysis

The gauge length of the electropolished tensile specimen of the weld metal was cathodically charged with hydrogen in a solution of 0.1N H_2SO_4 with 0.2 mg/L of As_2O_3 as poison. The solution was heated to 80°C (176°F) to promote

Table 1—Composition and Mechanical Properties of Weld Metal

Chemical analysis, wt-%:		
C	–	0.18
Mn	–	1.30
Si	–	0.19
S	–	0.02
P		0.005
Al	–	0.01
Mechanical properties:		
0.2% P.S., MPa		380
Tensile strength, MPa		543
Elongation, %		22.0

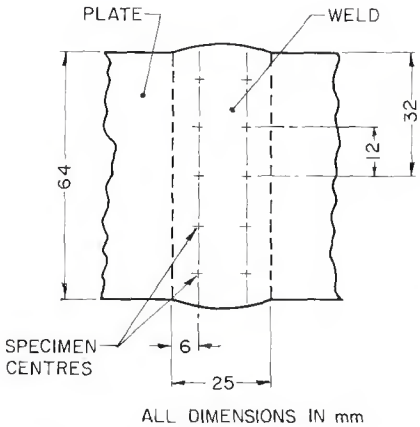

Fig. 1—Section of ESW normal to welding direction indicating location of tensile specimens

Table 2—Hydrogen Analyses of Broken Tensile Specimens

Current density i, mA/cm^2	Hydrogen level C_H, ppm
5	0.9 ± 0.5
25	2.7 ± 0.5
50	6.8 ± 1.0

hydrogen diffusion and homogenization, and was continuously stirred.

In a previous study on HSLA steel it was found that for this specimen size and charging conditions, homogenization occurred in 2 hours (h) (Ref. 8). Specimens were charged for this time at current densities of 5, 25 and 50 mA/cm^2 to obtain a range of hydrogen levels ($\sim$1, $\sim$3, and $\sim$8 ppm respectively). Hydrogen content was measured by cutting out the gauge section with an abrasive wheel and extracting the hydrogen by heating under vacuum; care was taken not to lose any hydrogen during handling. Three sets of test specimens were charged, and immediately stored in liquid nitrogen until tested.

Tensile testing

Tensile tests of both charged and uncharged specimens were performed at a nominal strain rate of $3.7 \times 10^{-4} s^{-1}$ on an Instron testing machine, at temperatures between −100 and 135°C (−148 and 275°F). The test temperatures were obtained by immersing specimens in heated baths of nitrogen-agitated heavy oil for testing above ambient temperature, and nitrogen-agitated methylbutane immersed in a bath of boiling liquid nitrogen for tests between 0 and −100°C (32 and −148°F). Charged specimens tested above ambient temperature were electroplated with a thin layer of cadmium to prevent hydrogen loss during testing.

The reduction in area of the fracture surface was calculated from measurements on the specimens, using a binocular microscope. Hydrogen determination by vacuum extraction was made for each condition of charging, using half of each broken tensile specimen. The average values are given in Table 2. Some uncharged specimens were analyzed to check for residual hydrogen in the as-welded metal; the result was zero ±0.5 ppm.

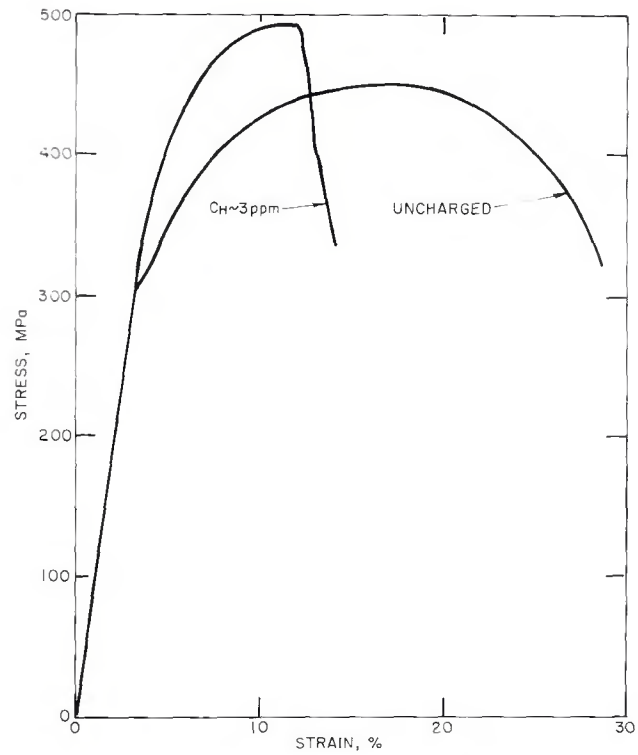

Fig. 2—Stress-strain curves of charged and uncharged specimens at test temperature 90°C (194°F)

Metallography

The microstructure of the ESW metal was examined both by optical microscopy and SEM. Selected fractures were examined by SEM. Longitudinal sections of some broken tensile specimens were also examined by optical microscopy and SEM.

Experimental Results

Tensile tests

The effect of hydrogen on the stress-strain curve of the ESW metal is shown in Fig. 2. The effect of hydrogen content and test temperature on reduction in ductility as measured by the true fracture strain (ϵ_f) is shown in Fig. 3. It is evident that with increasing hydrogen content (C_H) there is an increase in ductility loss and a widening of the temperature range where hydrogen embrittlement occurs in the ESW metal.

The effect of 3 ppm hydrogen on yield and flow stresses is shown in Fig. 4. Hydrogen increases both stress levels, at least over the temperature range shown. Other hydrogen contents give similar results, although the scatter is greater at $C_H \sim 1$ ppm.

Metallography

The microstructure of the ESW metal consists of pro-eutectoid ferrite; this outlines the prior austenite (γ) grain-boundaries, and acicular ferrite/pearlite within the massive (columnar) prior γ grains—Fig. 5. Cross sections of tensile specimens were found to contain a minimum of three prior γ grains.

SEM examination revealed that the constituents unresolved optically, primarily near prior γ grain-boundaries (Fig. 5B), are mainly pearlite colonies containing fine lamellae—Fig. 6A. This indicates that the pearlite has formed at low temperatures in spite of the low cooling rate of the ESW weld. Pearlite nucleation has likely been inhibited by the large grain size of the parent austenite. SEM examination also showed that the acicular ferrite in the prior γ grains were interspaced with carbide lamellae—Fig. 6B. The MnS inclusions were of globular shape, randomly distributed in the weld metal.

All uncharged specimens had ductile fractures. SEM fractography showed non-metallic inclusions at the bottom of some microvoids, which is a common feature of fracture by microvoid coalescence. SEM fractography of hydrogen-charged specimens ($C_H \sim 1$ ppm) showed the following as test temperature is increased:

1. At −50°C (−58°F), hydrogen-assisted "quasi-cleavage" facets originate at inclusions (Fig. 7A), and the final fracture occurs by shear failure at an angle to the tensile axis,
2. At 0°C (32°F), the fracture was

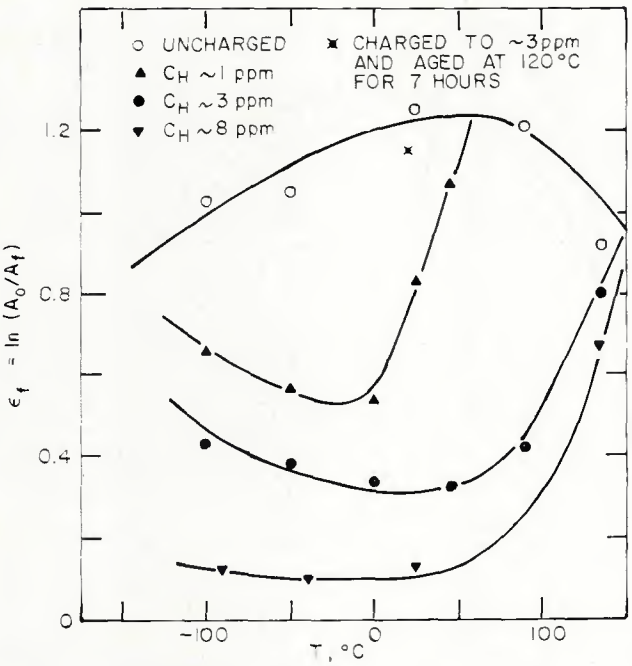

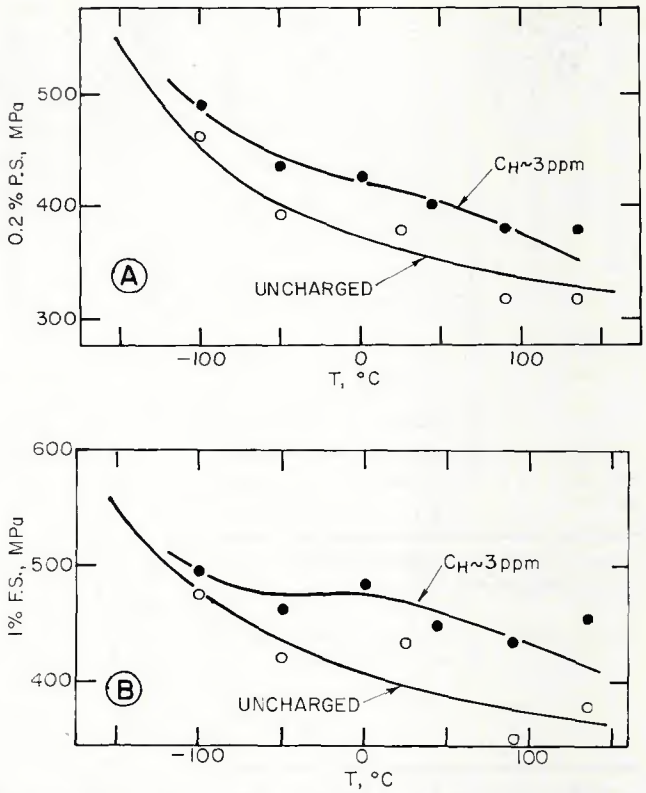

Fig. 3 — Effect of test temperature T and hydrogen content C_H on true fracture strain $\epsilon_f = \ln (A_o/A_f)$; A_o and A_f are initial and final cross-section areas, respectively

Fig. 4 (right) — Effect of test temperature T and hydrogen ($C_H \sim 3$ ppm) on: A — 0.2% proof stress (P.S.); B — 1% flow stress (F.S.)

primarily along prior γ grain-boundaries — Fig. 7B,

3. At 25°C (77°F), hydrogen-assisted microvoid coalescence — Fig. 7C.

Similar fracture modes were observed at larger C_H values, although the effect of hydrogen was more severe; the grain-boundary separation mode which gives maximum embrittlement was extended over a wider temperature range. Figure 8 shows a fracture where grain interior (region B) and grain-boundaries (region A) of the prior γ grains are clearly distinguished. SEM fractographs of the prior γ grain-boundaries (A) and the prior γ grains (B) of Fig. 8 are shown in Fig. 9. The fracture may be classified as of the "quasi-cleavage" type, i.e., predominantly cleavage accompanied by substantial plastic deformation evidenced by tear ridges.

Examination of longitudinal sections of broken tensile specimens confirmed that those with grain-boundary fractures predominant, had regions where the fracture path was along grain-boundary proeutectoid ferrite — Fig. 10A. Subsidiary crack formation is also evident, and shows preferential plastic deformation in these regions — Fig. 10B. SEM examination showed that the subsidiary crack paths in general appear to follow ferrite-pearlite or ferrite grain-boundaries — Fig. 11.

Discussion

Reduction in Ductility

The results given in Fig. 3 are shown in the form of an "embrittlement index" EI in Fig. 12 — that is, $EI = (\epsilon_{fu} - \epsilon_{fc})/\epsilon_{fu}$, where ϵ_f is true fracture strain, and subscripts u and c designate uncharged and charged conditions respectively. The limited temperature range of hydrogen embrittlement has been observed in mild (Ref 9), medium (Ref. 8, 10), and high strength (Ref. 11) steels. It has been ascribed by the present authors to decreased hydrogen transport at lower temperatures, and decreased hydrogen concentration at equilibrium in trap sites at higher temperatures (Ref. 8).

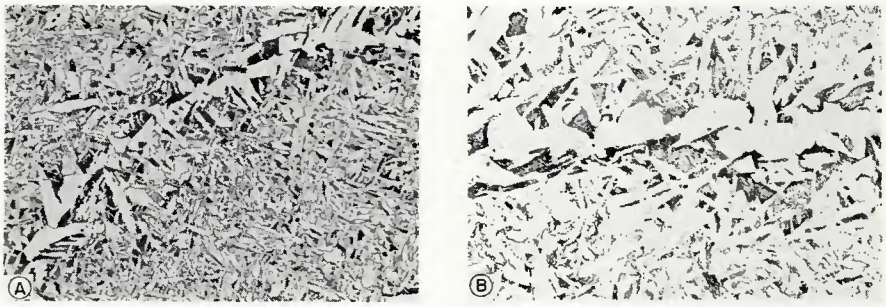

Fig. 5 — Microstructure of the ESW metal (normal to weld axis) etched with: A — nital, X250; and B — picral, X500 (A and B reduced 50% on reproduction)

In Figs. 3 and 12, the curve for $C_H \sim 8$ ppm suggests only limited recovery from embrittlement in the lower temperature range. It is quite possible that hydrogen concentration of this order can cause permanent damage. The general increase in EI with increase in C_H from ~ 1 ppm to ~ 8 ppm is consistent with the results of previous work on various steels and microstructures (Ref. 8, 9, 11). The reduction in ductility of the uncharged specimen tested at 135°C (275°F) (Fig. 3) is mainly due to dynamic strain-aging by carbon.

Figure 12 shows that in the ESW metal, the upper limit of the temperature range for embrittlement is 55°C (131°F) at $C_H \sim 1$ ppm and 145°C (293°F) at $C_H \sim 3$ ppm. Further increase in hydrogen level appears to increase this temperature only marginally. Recovery of ductility in the higher temperature range has been found to be independent of the strain rate, and hence hydrogen would not be expected to cause embrittlement above the upper limit at the corresponding C_H levels (Ref. 10, 12).

It may be deduced from these results that a hydrogen content of 1 ppm in the weld metal at ambient temperature can result in a form of delayed failure if sufficient restraint is present. The work of Boniszewski, *et al.* shows that hydrogen embrittlement as measured by the reduction in ductility in a slow tensile test at ambient temperature also causes delayed failure in a constant load rupture (CLR) test (Ref. 13). The CLR test is better than a slow tensile test at ambient temperature for comparing the susceptibility of similar microstructures, but it takes more time.

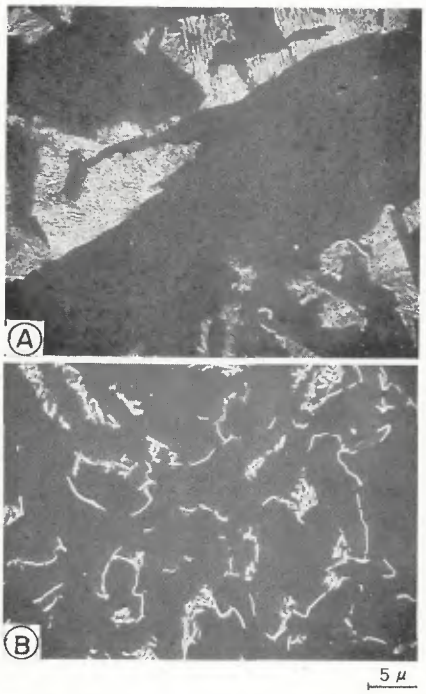

Fig. 6 — SEM micrographs: A — prior γ grain-boundary region; B — prior γ grain-interior

Also the results may be unreliable because of hydrogen loss during the test.

Figure 13 compares the embrittlement index curves for ESW metal with the results of a similar study (identical strain rate) on a HSLA direct-quenched steel (Ref. 8). It is clear that for comparable hydrogen levels the temperature of maximum embrittlement of the ESW metal is substantially higher — that is, at $C_H \sim 1$ ppm it is $\sim -10°C$ (14°F), while for the HSLA steel it is $\sim -80°C$ (−112°F) — Fig. 13A. The maximum embrittlement index is also higher for the weld metal at $C_H \sim 1$ ppm; however, this difference appears to decrease as C_H is increased — see Fig. 13 (note in Fig. 13B that C_H in the weld metal is lower than in the HSLA steel).

Clearly, hydrogen at low levels (~ 1 ppm) causes embrittlement near ambient temperature in the ESW metal. On the other hand, higher hydrogen levels are required for the HSLA steel which has good cold cracking resistance in the HAZ microstructure (Ref. 8, 14). Farrell and Quarrell made a similar study on a 0.35% high-strength steel with tensile strength of 1700 MPa (246.6 ksi) and an inherently high hydrogen susceptibility (Ref. 11). The results (with a strain rate $10^{-3}s^{-1}$) showed the temperature of maximum embrittlement to increase from $\sim -50°$ C (−58°F) at $C_H \sim 0.8$ ppm to 30°C (86°F) at $C_H \sim 1.3$ ppm compared to results in the present work: −10°C (14°F) at $C_H \sim 1$ ppm to 30°C (86°F) at $C_H \sim 3$ ppm.

Mechanisms of Embrittlement

It has been generally accepted that internal hydrogen embrittlement results

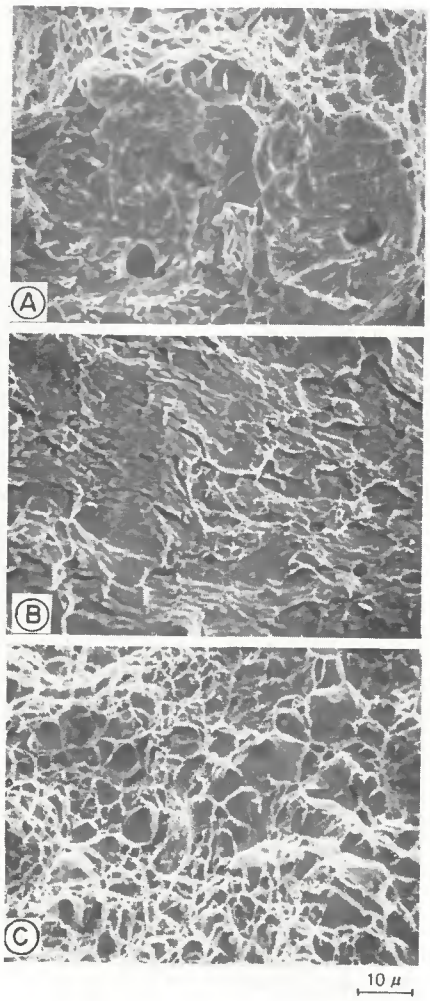

Fig. 7 — SEM fractographs of charged specimens ($C_H \sim 1$ ppm) tested at: A — minus 50°C (−58°F); B — 0°C (32°F); C — 25°C (77°F)

from hydrogen transport to susceptible sites such as inclusions, interfaces, grain boundaries, etc. However, it is now recognized that different mechanisms may operate depending on composition, microstructure, density and type of trap sites, and even test conditions, and that a unique "hydrogen fracture mode" does not exist (Ref. 2, 15).

In A36 steel, hydrogen increases both yield and flow stresses over the temperature range studied — Fig. 4. This effect is consistent with a hydrogen-dislocation interaction of the classic type with hydrogen atoms being dragged by mobile dislocations (Ref. 16). The possible transport of hydrogen by mobile dislocations to sites of fracture nucleation is discussed by Tien (Ref. 17); the other explanation for hydrogen transport is bulk diffusion.

The fractographic studies of this work showed three distinct forms of hydrogen-assisted fracture: quasi-cleavage facets nucleating at inclusions (Fig. 7A), prior γ grain-boundary separations (Fig. 7B), and hydrogen-assisted microvoid coalescence (Fig. 7C).

1. The quasi-cleavage facets observed around inclusions at test temperatures

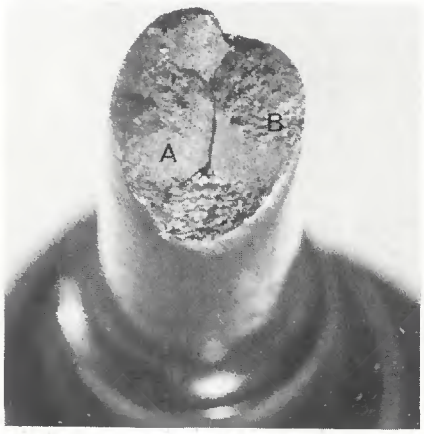

Fig. 8 — Fracture of a charged specimen ($C_H \sim 8$ ppm) tested at −40°C (−40°F)

below maximum embrittlement may be caused by hydrogen transport to inclusions. Subsidiary cracks formed at inclusions were found to be normal to the tensile axis and do not appear to follow any microstructural features.

2. The prior γ grain-boundary separations occurred at test temperatures which gave maximum embrittlement, (discussed in detail below under separate heading).

3. Hydrogen-assisted microvoid coalescence may occur by assisting either void nucleation which leads to a decreased dimple size or void growth which leads to increased dimple size (Ref. 18). No attempt was made in the present work to perform the extensive quantitative fractography to identify which mechanism operated in the present case.

The above fracture modes were found in specimens where cathodic charging caused no permanent damage (i.e., C_H up to 3 ppm) as confirmed by full recovery in ductility of an outgassed specimen (see Fig. 3).

Grain Boundary Separations

This feature was studied in depth, since it is the main form of cracking in electroslag weldments (Ref. 5, 7). In the present study, maximum embrittlement of the ESW metal was found when the fracture was primarily along prior γ grain-boundaries.

It has often been suggested in the past that in the presence of nonmetallic particles or films on boundaries, cracking can occur in weld metal during solidification, commonly known as "hot cracking" or "burning" (Ref. 1). Where the impurities are not at a sufficiently high level for this to occur, hydrogen cracks can occur along these boundaries. However, a recent study of electroslag welds has shown that prior γ grain-boundary separations are not related to solidification boundaries (Ref. 7). Microprobe analysis performed in the present work gave no evidence of impurity (sulphur or phos-

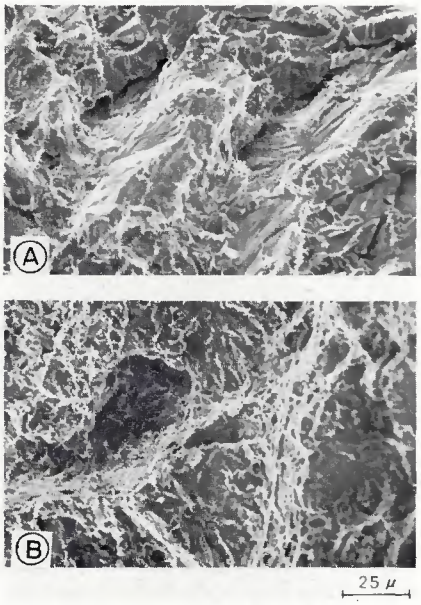

Fig. 9 — SEM fractographs of (A) prior γ grain-boundary, A, and (B) prior γ grain, B, in Fig. 8

phorus) segregation to the prior γ grain-boundaries.

When strong traps are present, such as in martensitic/bainitic structures, there is only partial recovery in ductility after mild degassing treatments (Ref. 8, 19); in contrast the ESW metal recovered fully after this treatment — Fig. 3. The increase in yield and flow stresses is evidence of hydrogen-dislocation interaction — Fig. 4. This effect was not observed in martensitic/bainitic structures because of the

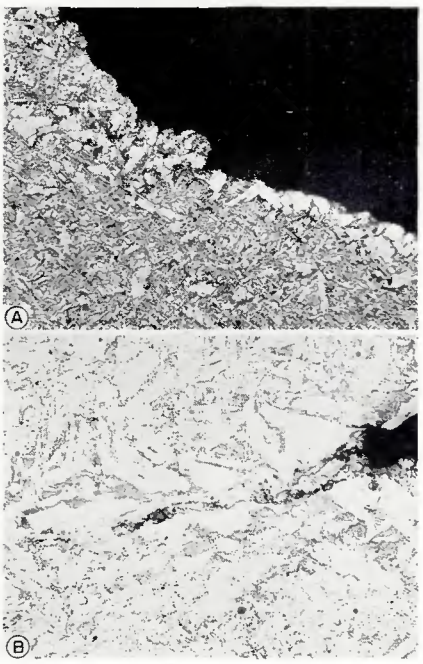

Fig. 10 — Optical micrographs of longitudinal sections of fractured specimens, charged to $C_H \sim 8$ ppm: A — tested at −40°C (−40°F), showing portion of the fracture profile, X200, B — tested at −90°C (−130°F), showing a subsidiary crack, X500 (A and B reduced 50% on reproduction)

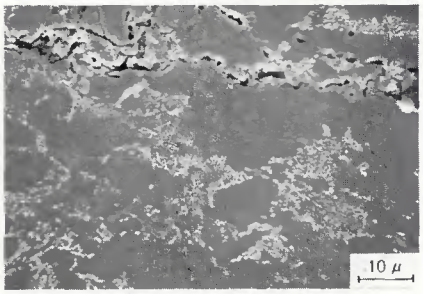

Fig. 11 — SEM micrograph of a grain-boundary separation in specimen with $C_H \sim 8$ ppm tested at −90°C (−130°F)

large density of trap-sites where most of the hydrogen is immobilized (Ref. 8). This suggests that most of the hydrogen is available for transport either by dislocations or bulk diffusion to sites of fracture nucleation in the ESW microstructure.

Fractography of the grain-boundary separations shows cleavage accompanied by substantial plastic deformation. In the grain-boundary regions containing the softer pro-eutectoid ferrite (Table 3) (Ref. 1, 5), preferential plastic deformation can occur under application of stress. As discussed earlier, hydrogen is available to diffuse to these regions when cracks form. Hence, grain-boundary separations can occur more readily with a microstructure having an inherently susceptible crack path in the grain-boundary pro-eutectoid ferrite and the adjacent pearlite, than with the more refined acicular ferrite/pearlite structure of the prior γ grain-interior — Fig. 5A. This supports the view that the effect of hydrogen increases where there are pre-disposed fracture paths (Ref. 3,15).

Crack paths of similar morphology following ferrite-pearlite boundaries were observed in banded line-pipe steels (Ref. 20). In this instance, however, the effect appears to be due to preferential hydrogen segregation. It should be noted that the coarse ferrite and pearlite grains outlining the prior γ grain-boundaries will

Table 3—Results of a Micro-Hardness Survey on ESW Metal

Region	Prior γ grain (acicular ferrite)	Prior γ grain-boundary (pro-eutectoid ferrite)
VHN	201	156

have a substantially higher fracture transition temperature than the relatively fine acicular ferrite/pearlite structure of the prior γ grain-interior. This could be a factor in causing embrittlement at higher temperatures than for the tougher HSLA steel at similar hydrogen concentrations (Fig. 13), because hydrogen-induced crack paths can control susceptibility (Ref. 3).

Of the factors that play a major role in forming cold cracks, it is clear that the microstructure of the ESW metal is responsible for cracks forming along prior γ grain-boundaries. Reduction of hydrogen sensitivity may be possible by refinement of the crack path microstructure, i.e., the grain-boundary pro-eutectoid ferrite region (Ref. 3), although this may not be sufficient to eliminate grain boundary separations.

Reducing the grain-boundary ferrite constituent of the weld metal microstructure may be achieved by lowering the $\gamma \rightarrow \alpha$ transformation temperature by either increasing the cooling rate or alloying (Ref. 21-23). The former is not a feasible method in this case. Alloying with elements such as Mn, Mo, Ni and Cr suppresses grain-boundary pro-eutectoid ferrite formation in favour of fine-grained structures in the prior γ grain-interior, such as acicular ferrite, and may be achieved with the same welding conditions (Ref. 22,23).* The commonly known low-hydrogen welding techniques or low external restraint can also be used. Low-hydrogen techniques have

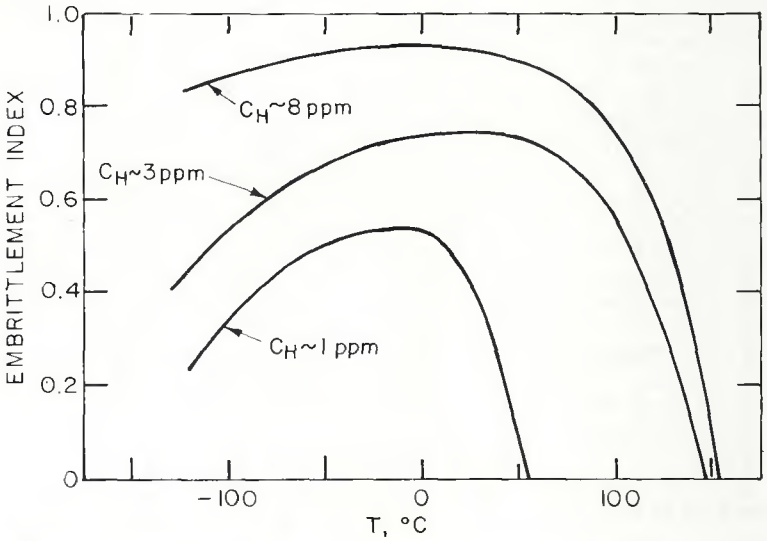

Fig. 12 — Variation of embrittlement index EI with test temperature T at $C_H \sim 1$, ~ 3, and ~ 8 ppm

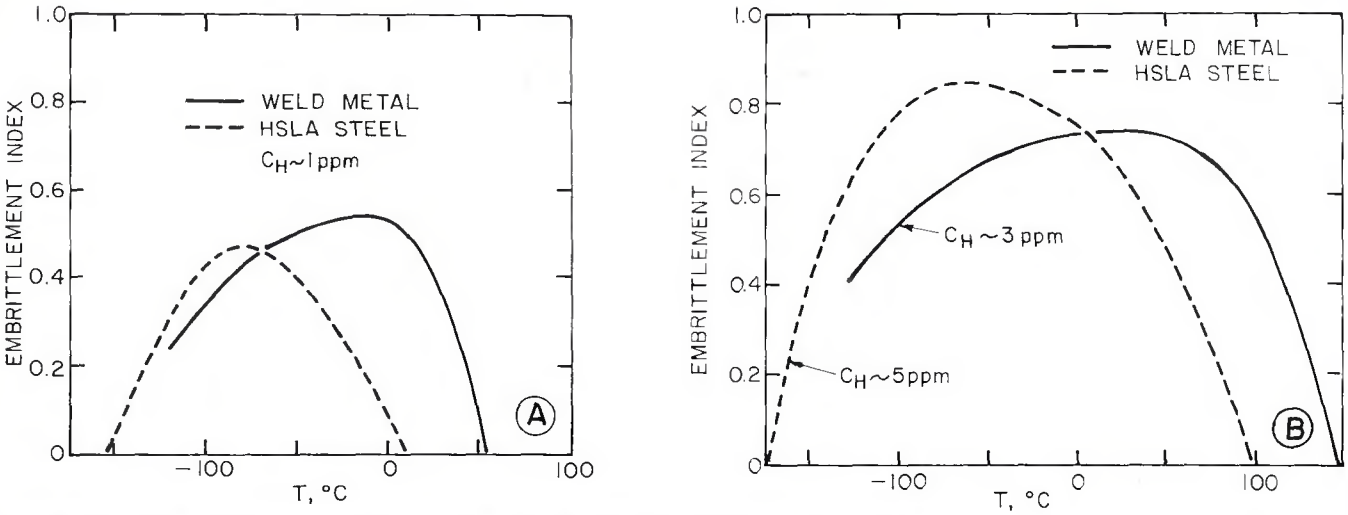

Fig. 13 — Comparison of EI curves for ESW metal (from Fig. 12) with those of HSLA direct-quench steel

been effective in eliminating grain-boundary separations in electroslag welds produced in the laboratory (Ref. 7).

Conclusions

The effect of internal hydrogen on the fracture behaviour of ESW metal obtained from a weldment of ASTM A36 steel plate, has shown the following:

1. At C_H of 1 and 3 ppm, the upper limits of the temperature range for hydrogen embrittlement are 55 and 145°C (131 and 293°F) respectively. Further increase in C_H only marginally increases this temperature. The temperature of maximum embrittlement is −10°C (14°F) at $C_H \sim 1$ ppm, and 30°C (86°F) at $C_H \sim 3$ ppm.
2. Three distinct modes of hydrogen-assisted fracture occur as test temperature is increased; these are: "quasi-cleavage" at inclusions, grain-boundary separation, and microvoid coalescence. The embrittlement index is largest for the grain-boundary separation mode.
3. At similar C_H values, the weld metal has a substantially higher temperature of maximum embrittlement than a HSLA direct-quenched steel (of low hydrogen susceptibility). Consequently, the upper limit of the temperature range for hydrogen embrittlement is higher than in the HSLA steel.
4. Slow strain-rate tensile tests confirm that hydrogen can cause prior γ grain-boundary separations, previously only observed in electroslag weldments.
5. Internal hydrogen increases both yield and flow stresses at temperatures where hydrogen embrittlement occurs.

Acknowledgments

The authors wish to thank NSERC and EMR of Canada for award of a Fellowship to L.N.P., and the staff at PMRL, EMR who have contributed to this work — in particular, Dr. J.D. Boyd for comments on the manuscript. We are also grateful to Dominion Bridge Co., Canada, for the material and information, and also for useful discussions.

References

1. Boniszewski, T., and Watkinson, F. 1973. Effect of microstructures on hydrogen-induced cracking in transformable steels. *Metals and Materials* 7 (2) and (3): 90-96 and 145-151.
2. Bernstein, I. M., and Thompson, A. W. 1976.(Dec.). Effect of metallurgical variables on environmental fracture of steels. *Int. Met. Revs.* 21 (4): 269-287.
3. Bernstein, I. M., and Thompson, A. W. 1976. Resisting hydrogen embrittlement. In *Alloy and microstructural design*, eds. J. K. Tien and G. S. Ansell: 303-347. New York: Academic Press.
4. Weintraub, P. 1978 (Dec. 25). Electroslag welded bridges called suspect. *American Metal Market/Metalworking News:* 8.
5. Kunihiro, T., and Nakajima, H. 1974. Microcracking in consumable-nozzle electroslag weld metal. *Proc. Japan — U. S. seminar on significance of defects in welded structures*: 105-109.
6. Nishio, Y.; Hiromoto, Y.; and Inoue, K. *Study of hydrogen behaviour and preventing method of weld crack in electroslag weld zones.* Int. Inst. of Welding document no. XII-J-48-76.
7. Konkol, P. J., and Domis, W. F. 1979. Causes of grain boundary separations in electroslag weld metals. *Welding Journal* 58 (6): 161-s to 167-s.
8. Pussegoda, L. N., and Tyson, W. R. 1979. *Hydrogen embrittlement of HSLA direct-quenched steel and its simulated microstructures.* PMRL report MRP/PMRL 79-73 (J), CANMET, Energy, Mines and Resources, Canada.
9. Toh, T., and Baldwin, W. M., Jr. 1956. Ductility of steel with varying concentrations of hydrogen. In *Stress corrosion cracking and embrittlement*, ed. W. D. Robertson: 176-186. New York: Wiley.
10. Tobe, Y., and Tyson, W. R. 1977 (June). Hydrogen embrittlement of a boron steel. *2nd int. congress hydrogen in metals* 10: 9 pp. Paris, France.
11. Farrell, K., and Quarrell, A. G. 1964. Hydrogen embrittlement of an ultra-high-tensile steel. *J Iron and Steel Inst.* 202 (12): 1002-1011.
12. Graville, B. A.; Baker, R. G.; and Watkinson, F. 1967. Effect of temperature and strain-rate on hydrogen embrittlement of steel. *Brit. Weld. J.* 14 (6): 337-342.
13. Boniszewski, T., *et al.* 1965. Hydrogen embrittlement and HAZ cracking in low-carbon alloy steels with acicular microstructures. *Brit. Weld. J.* 12 (1): 14-36.
14. Gordine, J. 1978 (May). *Weldability testing of a direct-quench line-pipe steel.* PMRL report ERP/PML 78-3 (IR). CANMET, Energy, Mines and Resources, Canada.
15. Bernstein, I. M., and Thompson, A. W. 1977. An evaluation of hydrogen embrittlement mechanisms. *Proc. Int. Conf.: mechanisms of environment sensitive cracking of materials*, eds. P. R. Swann, F. P. Ford, and A. R. C. Westwood: 412-425. London: Metals Society.
16. Tobe, Y., and Tyson, W. R. 1977. Effect of hydrogen on yield of iron. *Scripta Met.* 11 (10): 849-852.
17. Tien, J. K. 1976. Diffusion and dislocation sweeping mechanism for hydrogen transport. *Effect of hydrogen on behaviour of materials*, eds. A. W. Thompson and I. M. Bernstein: 309-326. New York: TMS-AIME.
18. Thompson, A. W. 1979. Ductile fracture topography: geometrical contributions and effects of hydrogen. *Met Trans.* 10A (6): 727-731.
19. Morris, J. G., and Roopchand, B. J. 1977 (Oct.). Metallurgical structures to resist hydrogen embrittlement in ferrous alloys. *Proc. of Conf.: environment degradation of engineering materials*, eds. M. R. Louthan Jr. and R. P. McNutt: 475-485. Blacksburg, Va.
20. Groeneveld, T. P., and Fessler, R. R. 1979. Hydrogen-induced damage in sour-gas gathering lines. Paper presented at NACE Western Region Conf., Feb. 1979, in Calgary, Alberta, Canada.
21. Glover, A. G., *et al.* 1977. The influence of cooling rate and composition on weld metal microstructures in a C-Mn and a HSLA steel. *Welding Journal* 56 (9): 267-s to 273-s.
22. Yoshino, Y., and Stout, R. D. 1979. Effect of microalloys on the notch toughness of line pipe seam welds. *Welding Journal* 58 (3): 59-s to 68-s.
23. Evans, G. M. 1980. Effects of manganese on the microstructure and properties of all-weld-metal deposits. *Welding Journal* 59 (3): 67-s to 75-s.